Engineering Science and Technology, an International Journal 24 (2021) 469–479

HOSTED BY

Contents lists available at ScienceDirect

Engineering Science and Technology, an International Journal

journal homepage: www.elsevier.com/locate/jestch

Full Length Article

Opposition-based artificial electric field algorithm and its application to FOPID controller design for unstable magnetic ball suspension system

Ayşen Demirören [a], Serdar Ekinci [b,*], Baran Hekimoğlu [c], Davut Izci [d]

[a] Department of Electrical Engineering, Istanbul Technical University, Istanbul 34469, Turkey
[b] Department of Computer Engineering, Batman University, Batman 72100, Turkey
[c] Department of Electrical & Electronics Engineering, Batman University, Batman 72100, Turkey
[d] Vocational School of Technical Sciences, Batman University, Batman 72060, Turkey

ARTICLE INFO

Article history:
Received 3 May 2020
Revised 30 June 2020
Accepted 2 August 2020
Available online 28 August 2020

Keywords:
Artificial electric field algorithm
Optimization
Magnetic ball suspension system
Magnetic levitation (maglev)
Fractional order PID controller
Opposition-based learning

ABSTRACT

In this study, an improved version of artificial electric field (AEF) algorithm, named as opposition-based AEF (ObAEF), has been proposed for the first time ever to tune a fractional order PID (FOPID) controller used in a magnetic ball suspension system. The basic AEF algorithm is a novel physics-inspired, population-based meta-heuristic optimization method that mathematically mimics Coulomb's electrostatic force between charged particles. The proposed ObAEF algorithm is the improved version of the AEF which utilizes the opposition-based learning strategy to enhance the AEF algorithm's exploration capability. To validate the performance, the novel ObAEF algorithm was applied to 6 well-known benchmark optimization problems of Sphere, Rosenbrock, Schwefel, Ackley, Egg Crate and Easom. The results were also compared with other algorithms such as basic AEF, atom search optimization (ASO) and artificial bee colony (ABC). It was also used to tune FOPID controller (ObAEF-FOPID) to improve the transient response of a magnetic levitation (maglev) system by minimizing a new objective function having a simple structure. The latter was proposed to minimize the maximum overshoot, settling and rise times along with steady state error of magnetically suspended ball's position. The convergence profile and statistical analyzes were conducted to illustrate the success of the proposed algorithm. The effectiveness and superiority of the ObAEF-FOPID controller was further investigated through frequency response analysis and again compared with AEF, ABC and ASO based FOPID controllers as in statistical success, convergence profile and transient analyses. The results showed that the proposed ObAEF-FOPID has better control performance than those tuned by AEF, ASO and ABC algorithms.
© 2020 Karabuk University. Publishing services by Elsevier B.V. This is an open access article under the CC BY-NC-ND license (http://creativecommons.org/licenses/by-nc-nd/4.0/).

1. Introduction

The interaction between a magnetic object and applied magnetic field can be utilized to lift or suspend objects. This process is known as magnetic levitation (maglev). Maglev systems are used in many engineering applications such as high-speed elevators [1], passenger trains [2], vibration isolation systems [3] and minimal invasion surgery [4]. The dynamic adjustment of electromagnet (s) in the system may be necessary to fix the magnetized object in a desired position. An electronic feedback control is required to stabilize a levitated magnetic object due to non-linear and unstable nature of the maglev system. To do so, proportional-integral-derivative (PID) [5] or fractional order PID (FOPID) [6] controllers can be utilized to keep a magnetic object at a fixed position and provide stabilization. The conventional PID controllers are widely used in control systems, especially industrial applications, due to its easy implementation, robustness and simplicity [7,8]. The FOPID controllers, on the other hand, are the extended version of the conventional PID controller with two additional fractional order parameters (λ, μ) [6] and can provide better performance.

Instead of classical methods such as phase-gain margin and pole placement, the use of meta-heuristic algorithms for tuning the parameters of PID and FOPID controllers to their best values has increasingly become widespread [9,10]. There are examples of tuning PID and FOPID controllers for maglev systems using meta-heuristic algorithms such as two degree-of-freedom PID controller using pole search technique by utilizing particle swarm optimization (PSO) algorithm [11], which was compared with the

* Corresponding author.
E-mail addresses: demiroren@itu.edu.tr (A. Demirören), serdar.ekinci@batman.edu.tr (S. Ekinci), baran.hekimoglu@batman.edu.tr (B. Hekimoğlu), davut.izci@batman.edu.tr (D. Izci).

Peer review under responsibility of Karabuk University.

https://doi.org/10.1016/j.jestch.2020.08.001
2215-0986/© 2020 Karabuk University. Publishing services by Elsevier B.V.
This is an open access article under the CC BY-NC-ND license (http://creativecommons.org/licenses/by-nc-nd/4.0/).

conventional and nonlinear interior point optimization based 1- and 2- degree-of-freedom PID and FOPID controllers [12,13] and Jaya optimization based I-PD controller [14] designed for the same maglev plant. Further examples can be listed as PID controller designed by utilizing bat algorithm (BA) [15] and teaching learning based optimization (TLBO) [16], discrete optimal pole-zero approximation to implement a digital fractional order controller using dynamic PSO [17]. In addition, PSO and gravitational search algorithm (GSA) along with hybrid version of these two algorithms [18] with genetic algorithm (GA) [19] was proposed for tuning both PID and FOPID controllers in a maglev system. Simulation and experimental results verified the effectiveness of the proposed digital FOPID controller compared to conventional PD and PID controllers. It was noticed that, to obtain the same system performance, fractional order control requires less effort than its integer counterparts. The simulation results confirmed the FOPID controller to be better than that of conventional PID in terms of rise time, overshoot and settling time.

The main goal of all studies mentioned so far was to achieve an improved control system performance for maglev systems in terms of transient and frequency responses. Studying novel meta-heuristic optimization algorithms is of importance to achieve the improved system dynamics with better performance characteristics. Therefore, in this paper, artificial electric field (AEF) algorithm has been decided to be employed for maglev system. There is no application of AEF algorithm in the previous related works on maglev system. This algorithm is a new physics-inspired population-based meta-heuristic optimization method, which mathematically mimics the Coulomb's electrostatic force and Newton's motion laws [20]. This algorithm has already been applied to 28 constrained benchmark problems, and five nonlinear multidimensional structural design optimization problems in order to demonstrate the efficiency [21]. It was also extended as a discrete AEF algorithm for combinatorial high-order graph matching problems [22]. The latter study also showed that this algorithm can outperform many state-of-the-art algorithms.

However, as with any meta-heuristic algorithm, there are weaknesses of this algorithm such as local minima stagnation and poor exploration capability. To avoid such drawbacks, opposition-based learning (OBL) strategy was used to establish a candidate solution with the opposite position in the search space [23]. This allows two-way exploration at the same time in the search space. OBL selects the best elements from both candidate and opposing solutions with the aid of objective function values. The OBL rule can be not only used at the start of meta-heuristic algorithms but also at any part of algorithm where a solution is modified. Using OBL, different meta-heuristic algorithms have been improved, which yielded better results than their standard versions. An example of these improvements is the opposition-based sine cosine algorithm where OBL helped increasing the convergence rate of sine cosine algorithm (SCA) [24]. OBL was also used for parameter estimation of solar cell diode models [25] and feature selection [26], respectively. The OBL combination has also been extended for engineering applications, in which the problem of economic load distribution has been addressed by opposition-based grey wolf optimization (GWO) [27]. In addition, the opposition-based dragonfly algorithm (DA) has recently been introduced as an alternative approach to engineering problems [28]. Further examples of hybridized OBL based works can be listed as opposition theory enabled moth flame optimizer (MFO) to solve strategic bidding problem [29], improved version of salp swarm algorithm (SSA) to solve feature selection problems [30], atom search optimization (ASO) algorithm to tune PID + DD controller parameters for automatic voltage regulator (AVR) system [31] along with intelligent crow search algorithm (CSA) to avoid local minima stagnation and improve unbalanced exploration and exploitation phases in standard CSA [32]. All these studies show that OBL can be utilized to achieve better results.

In this study, the success of the OBL-based AEF (ObAEF) algorithm has been verified on benchmark functions of Sphere, Rosenbrock, Schwefel, Ackley, Egg Crate and Easom. Besides, the ObAEF algorithm has also been proposed to tune FOPID controller in a maglev system, in particular by means of a new objective function having a simple structure. The latter was used to improve settling time and overshoot as much as possible. The performance and advantage of the proposed ObAEF-based FOPID controller have been verified through convergence, statistical, transient and frequency response analyses. Comparisons of ObAEF-FOPID controller with AEF-FOPID, ASO-FOPID and artificial bee colony (ABC) based FOPID (ABC-FOPID) controllers have been made in terms of transient response and frequency response analyzes. The contributions of this paper can be summarized as follows:

- The ObAEF algorithm was proposed for the first time.
- The proposed ObAEF algorithm has been applied to the optimization problem of 6 well-known benchmark functions. The obtained results were compared with other algorithms such as ASO and ABC as well as AEF.
- The proposed ObAEF and AEF algorithms were both used for the first time ever in design of FOPID controller of a maglev system.
- It was also proposed to use a new and effective objective function with a simpler structure in combination with the ObAEF tuned FOPID controller, thereby maximizing the dynamic performance of the maglev system.
- The performance of the proposed ObAEF-FOPID approach was compared in detail with AEF-FOPID, ASO-FOPID and ABC-FOPID controllers and the comparative statistical success, convergence profile, transient response and frequency response analyses were clearly confirmed the effectiveness of the proposed approach and its superiority over other algorithms.

2. Opposition based artificial electric field (ObAEF) algorithm

2.1. The basic AEF algorithm

Coulomb's electrostatic force law states that a force occurs between charged particles which have a proportional relationship with the product of their charges. This force has also an inversely proportional relationship with the square of the distance between charges. This has inspired the AEF algorithm where the search agents are considered to be charged particles and the strengths of them are measured by the charges they have [20]. Particles can move in the search space since they can repel or attract each other by the electrostatic force. That means a charged particle communicates with other particles through the electrostatic force and its position corresponds to a solution in the solution space. In AEF algorithm, only the attraction force is considered, meaning that a charged particle with strongest charge ("best" individual) attracts all particles with lower charge. In this way, it can move slowly in the search space. The construction of the AEF algorithm is explained as follows using Coulomb's electrostatic force and Newton's motion laws. The position of particle i (X_i) at time t is given as in Eq. (1)

$$X_i(t) = \left(X_i^1, X_i^2, \cdots, X_i^D\right), \quad i = 1, 2, \cdots, N \text{ and } d = 1, 2, \cdots, D \tag{1}$$

where total number of charged particles are denoted by N and total number of parameters are denoted by D. The position of particle i that achieve the best fitness value at any time t is given as in Eq (2).

$$P_i^d(t+1) = \begin{cases} X_i^d(t+1) \text{ if } f(X_i(t+1)) \le f(P_i(t)) \\ P_i^d(t) \text{ if } f(X_i(t+1)) > f(P_i(t)) \end{cases} \tag{2}$$

The position of the particle with the best fitness is denoted by $P_{best} = X_{best}$. The force acting on particle i due to particle j at time t is defined as given in Eq. (3)

$$F_{ij}^{d}(t) = K(t)\frac{Q_i(t)\cdot Q_j(t)\cdot (P_j^d(t) - X_i^d(t))}{R_{ij}(t)+\varepsilon} \tag{3}$$

where $Q_i(t)$ and $Q_j(t)$ are the charges of particle i and particle j at time t. $K(t)$, ε and $R_{ij}(t)$ represent the Coulomb's constant, a small positive constant and the Euclidean distance between two particles which is given as in Eq. (4).

$$R_{ij}(t) = \|X_i(t), X_j(t)\|_2 \tag{4}$$

The term $K(t)$ is calculated as a function of iteration and the maximum iteration as provided in Eq. (5)

$$K(t) = K_0 \cdot e^{(-\alpha\frac{iter}{maxiter})} \tag{5}$$

where α is a parameter and equals 30, K_0 (equals 500), max*iter* and *iter* are the initial value, predetermined maximum number of iterations and current iteration, respectively. The constant K_0 is initialized at the beginning of the algorithm with a big value to allow a better exploration. It is then decreased through iterations to control the search accuracy. The total electric force acting on particle i at time t in dimension d is given in Eq. (6)

$$F_i^d(t) = \sum_{j=1, j\neq i}^{N} rand\cdot F_{ij}^d(t) \tag{6}$$

where F_i^d is the resultant force acting on charged particle i at time t in dimension d. *rand* stands for a uniformly generated random number having range of [0,1]. The latter random number has the role to provide the stochastic nature. The electric field of the charged particle i at time t in dimension d is given in Eq. (7).

$$E_i^d(t) = \frac{F_i^d(t)}{Q_i(t)} \tag{7}$$

The acceleration of particle i at time t in dimension d is given in Eq. (8) by using Eq. (7) and Newton's law of motion.

$$a_i^d(t) = \frac{Q_i(t)\cdot E_i^d(t)}{M_i(t)} \tag{8}$$

In the latter equation, $M_i(t)$ represents the unit mass of particle i at time t. Eq. (9) and (10) are used to update the velocity and the position of the particle, respectively,

$$V_i^d(t+1) = rand\cdot V_i^d(t) + a_i^d(t) \tag{9}$$

$$X_i^d(t+1) = X_i^d(t) + V_i^d(t+1) \tag{10}$$

where *rand* stands for a uniformly generated random number having range of [0,1]. The particle charges are calculated as in Eq. (11) by assuming equal charge for each particle.

$$Q_i(t) = Q_j(t) = \frac{q_i(t)}{\sum_{i=1}^{N} q_i(t)} \quad i,j = 1,2,\cdots,N \tag{11}$$

In Eq. (11), $q_i(t)$ stands for a suitable charge function chosen to yield the largest normalized value for the best particle ($Q_{best} = 1$), and is calculated as in Eq. (12)

$$q_i(t) = e^{\left(\frac{fit_i(t)-worst(t)}{best(t)-worst(t)}\right)} \tag{12}$$

where $fit_i(t)$ is the fitness value of particle i at time t, $best(t)$ is fitness value of the best particle and $worst(t)$ is fitness value of the worst particle, and they are defined as given in Eq. (13) for a minimization problem.

$$\begin{aligned} best(t) &= min(fit_i(t))\ i \in (1,2,\cdots,N) \\ worst(t) &= max(fit_i(t))\ i \in (1,2,\cdots,N) \end{aligned} \tag{13}$$

AEF algorithm's flow chart is illustrated in Fig. 1. As seen from the flowchart, the algorithm starts with randomly initializing the particles. Then, for each iteration, the fitness of each particle is evaluated, and the fitness values of the best and worst particles are calculated. In the next step of the iteration, the velocities and the positions of each particle is updated. This process is repeated until the maximum number of iterations, and consequently, the obtained best solution is provided.

2.2. Opposition-based optimization approach

The basic AEF suffers from slow convergence and being trapped in a local best solution. These disadvantages are caused by updating some solutions towards the local best solution although there may be some better solutions that are away from current solution. The ObAEF avoids those disadvantages by considering opposite solutions. In addition, the exploration efficiency of the search space is increased by combining standard version of AEF's search capabilities with OBL. Fewer parameters are required to be set with the proposed approach since the inclusion of OBL does not affect the AEF configuration, thus, the accuracy of the best solution increases whilst compared to similar algorithms. Since ObAEF can explore the search space more widely, reducing the initial population's size

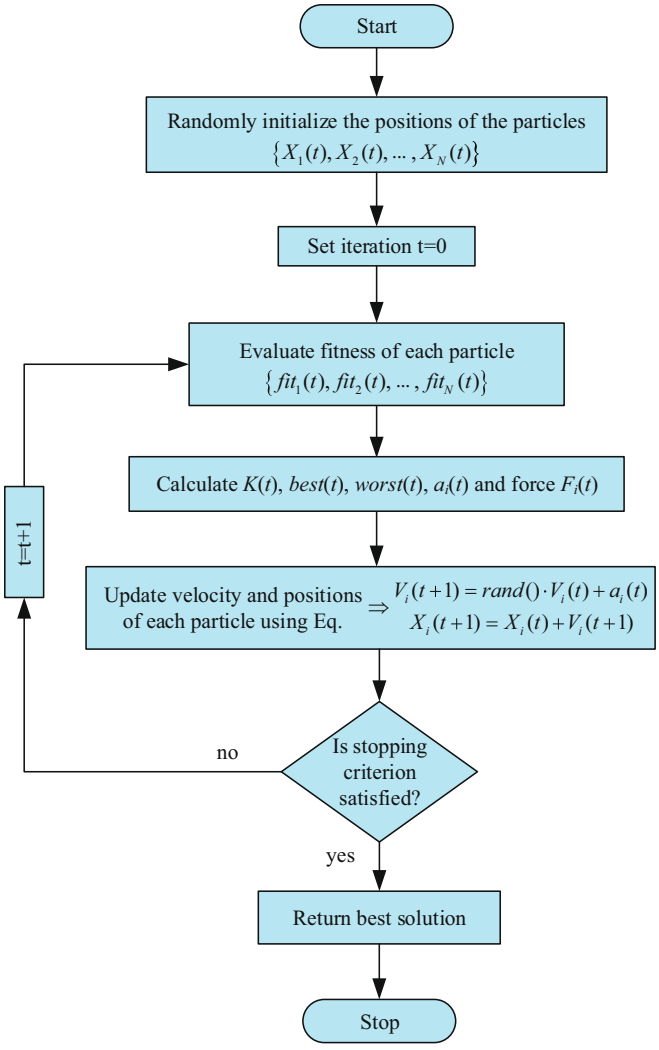


Fig. 1. AEF algorithm's flow chart [20].

is possible which leads to improvement of the optimal solution convergence.

AEF is improved in two stages with the proposed algorithm. Firstly, OBL is used to initiate the population to increase convergence speed and to avoid trapping the local best solution by searching for solutions across the entire search space. Secondly, it is used to update the population solution and to check whether the updated solution in the opposite direction is better than the current one. Both steps are described in following sub-sections.

2.2.1. Initialization stage

The proposed method begins with the generation of a random population of X (having size of N) such that the position vector of the initial solution is expressed by $X_i = \left[X_i^1, X_i^2, \cdots, X_i^D\right]$ where $i = 1, 2, \cdots, N$ and $d = 1, 2, \cdots, D$. After that, OBL calculates the opposite solution for each solution and then the opposite population of $\overline{X}$ is generated. The best N number of solutions are selected based on X and $\overline{X}$. The steps can be listed as follows for this stage.

- Solutions of X population are randomly initialized.
- The opposite population $\overline{X}$ ($\overline{X}_i^d = u^d + l^d - X_i^d$, $i = 1, 2, \cdots, N$ and $d = 1, 2, \cdots, D$) is calculated where u is the upper bound and l is the lower bound of the search space, X_i^d and $\overline{X}_i^d$, represent the position of the d th parameter of the i th solution in population X and the corresponding opposite solution in population $\overline{X}$, respectively.
- The best N solutions from the combination of $X \cup \overline{X}$ are chosen to create a new population.

2.2.2. Updating stage

After choosing best N solutions from a new population, the best solution X_{best} is determined. AEF is used to update the solutions in the X population and calculate their fitness functions. In addition, the opposite $\overline{X}$ population obtained according to OBL and their fitness functions are also calculated. The next step is to select the best N number of solutions from the union set of $X \cup \overline{X}$ according to their fitness functions. All steps are repeated until satisfaction of the termination conditions. The proposed ObAEF algorithm is shown in Fig. 2.

Benchmark functions of Sphere, Rosenbrock, Schwefel, Ackley, Egg Crate, and Easom were utilized for performance verification of ObAEF algorithm. Table 1 provides a summary of adopted test functions definitions. The reader is referred to refs. [33,34] for detailed information on these functions. The population size was chosen to be 50 whereas maximum iteration number was selected as 500. The proposed ObAEF algorithm was run 20 times to have an appropriate comparison with other algorithms such as ABC, ASO and AEF. The ABC [33] is a nature inspired meta-heuristic algorithm whereas ASO [34] is of physics inspired. In ABC, the intelligent behavior of honeybee swarms is employed by following workload sharing strategies which consequently helps the exploration and exploitation processes to be performed. In ASO, the atomic motion is modelled mathematically by considering the interaction forces occurring between atoms. It is to implement the latter algorithm to optimization problems due to fewer control parameters it has.

The statistical results of the relevant test functions such as best, worst, mean and standard deviation (SD) are demonstrated in Table 2. As clearly seen, ObAEF achieved the best results compared to standard AEF and other algorithms. Due to superior success of ObAEF algorithm in solving test functions, it was proposed for one of the challenging real-world engineering problems known as magnetic levitation control system.

2.3. Computational complexity of ObAEF

The computational complexity of AEF mainly consists of three parts; initialization, fitness evaluation and population updating which can be calculated as $O(\text{AEF}) = O(N) + O(N \times T) + O(N \times D \times T)$. In here, N, D and T represent the population size, dimension of the problem and maximum number of iterations, respectively. The complexity of AEF would increase with the application of OBL method. In each iteration, OBL performs operations on N individuals to produce N opposite individuals and the algorithm calculates the fitness value of $2N$ individuals. After ranking $2N$ fitness values, the best N individuals would be selected to continue updating. Therefore, the entire computational complexity of ObAEF would be $O(\text{ObAEF}) = O(2N) + O(2N \times T) + O(2N \times D \times T)$. That means the computational complexity of ObAEF is obviously higher than that of the basic AEF.

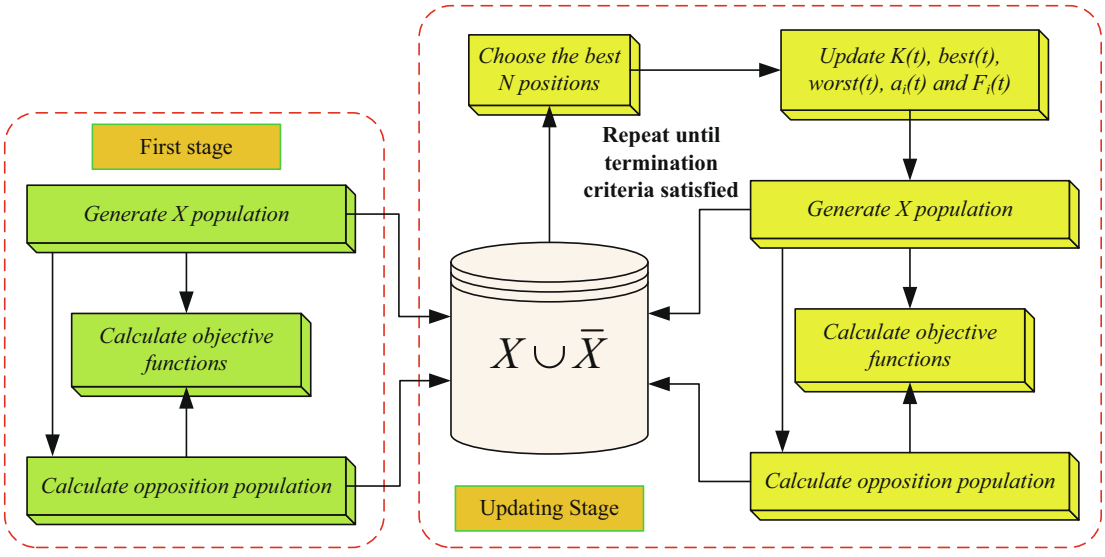


Fig. 2. Structure of the proposed ObAEF algorithm.

Table 1
Some benchmark functions.

Test Function	Function Definition	Dimension	Range	Global Optimum
Sphere	$F_1(x) = \sum_{i=1}^{D} x_i^2$	$D = 30$	$-100 \le x_i \le 100$	0
Rosenbrock	$F_2(x) = \sum_{i=1}^{D-1}\left[100(x_{i+1} - x_i^2)^2 + (x_i - 1)^2\right]$	$D = 30$	$-30 \le x_i \le 30$	0
Schwefel	$F_3(x) = -\sum_{i=1}^{D} x_i \sin(\sqrt{\lvert x_i \rvert})$	$D = 30$	$-500 \le x_i \le 500$	−12569.487
Ackley	$F_4(x) = -20\exp\left(-0.2\sqrt{\frac{1}{D}\sum_{i=1}^{D} x_i^2}\right) - \exp\left(\frac{1}{D}\sum_{i=1}^{D}(\cos(2\pi x_i))\right) + 20 + e$	$D = 30$	$-32 \le x_i \le 32$	0
Egg Crate	$F_5(x) = x_1^2 + x_2^2 + 25\left[sin^2(x_1) + sin^2(x_2)\right]$	$D = 2$	$-5 \le x_i \le 5$	0
Easom	$F_6(x) = -\cos(x_1)\cos(x_2)exp\left(-(x_1 - \pi)^2 - (x_2 - \pi)^2\right)$	$D = 2$	$-100 \le x_i \le 100$	−1

Table 2
Results obtained from comparison of various benchmark functions.

Test Function	Index	ABC	ASO	AEF	ObAEF (Proposed)
Sphere	Mean	2.0710E-05	3.2561E-19	1.1309E-22	**1.3933E-53**
	SD	2.5654E-05	2.8231E-19	3.3287E-22	**3.2757E-53**
	Best	3.1200E-06	1.1800E-20	9.8230E-25	**0**
	Worst	1.1100E-04	8.4500E-19	1.1798E-21	**1.2348E-52**
Rosenbrock	Mean	33.7430	26.3785	24.9728	**0.3389**
	SD	29.3305	0.6498	4.8439	**0.4846**
	Best	1.2002	24.2918	18.5805	**1.7534E-05**
	Worst	99.0436	27.3008	34.2049	**1.7747**
Schwefel	Mean	−1.1522E+04	−7.4040E+03	−1.0016E+04	**−1.2541E+04**
	SD	154.0439	778.3425	1.2791E + 03	**37.5594**
	Best	−1.1902E+04	−8.5822E+03	−1.1983E+04	**−1.2569E+04**
	Worst	−1.1265E+04	−6.1731E+03	−7.3856E+03	**−1.2457E+04**
Ackley	Mean	0.1001	4.5684E-10	1.0843E-12	**1.1686E-14**
	SD	0.0939	3.4200E-10	2.8998E-13	**4.2635E-15**
	Best	0.0135	3.5800E-11	6.5959E-13	**5.7358E-15**
	Worst	0.3610	1.3400E-09	1.8124E-12	**2.0645E-14**
Egg Crate	Mean	1.2596E-18	2.8316E-24	1.7021E-26	**1.7265E-87**
	SD	1.3255E-18	3.6095E-24	1.8298E-26	**5.1910E-87**
	Best	4.8400E-21	0	3.5025E-27	**0**
	Worst	5.0500E-18	1.3100E-23	7.9372E-26	**1.8329E-86**
Easom	Mean	−1.0000	−3.1865E-06	−0.7521	**−1.0000**
	SD	0	1.1291E-05	0.1528	**0**
	Best	−1.0000	−4.9200E-05	−0.9268	**−1.0000**
	Worst	−1.0000	−9.8700E-142	−0.2899	**−1.0000**

3. Magnetic ball suspension system

A magnetic suspension system is a maglev system for lifting and suspending a ferromagnetic object through magnetic field without contacting it. The purpose of the system is to change the current of an electromagnet using an input voltage $v(t)$ and to control the position of the ferromagnetic object such as a steel ball. The schematic diagram of the suspension system of a magnetic ball is shown in Fig. 3. In this system, the input current of the coil acting as an electromagnetic actuator so that the upward electromagnetic force on the ball is equal to the weight of that ball. In this way, the ball remains in balance. It is difficult to control a magnetic suspension system since it is fast, dynamic, and non-linear unstable system. Therefore, it must be stabilized with a feedback control system.

The dynamic behavior of magnetic levitation system can be modeled by examining the electromagnetic and mechanical subsystems. The net force acting on the ball (according to Newton's second law) is given in Eq. (14) [35]

$$M\frac{d^2y(t)}{dt^2} = M \cdot g - k\frac{i^2(t)}{y(t)} \tag{14}$$

where, M is the mass of the ball, k is the electromagnet coefficient, g is the gravitational acceleration. $i(t)$ stands for the winding current whereas $y(t)$ is the ball position. According to Kirchoff's voltage law, the relationship between the input voltage and the coil current can be written as in Eq. (15) [35].

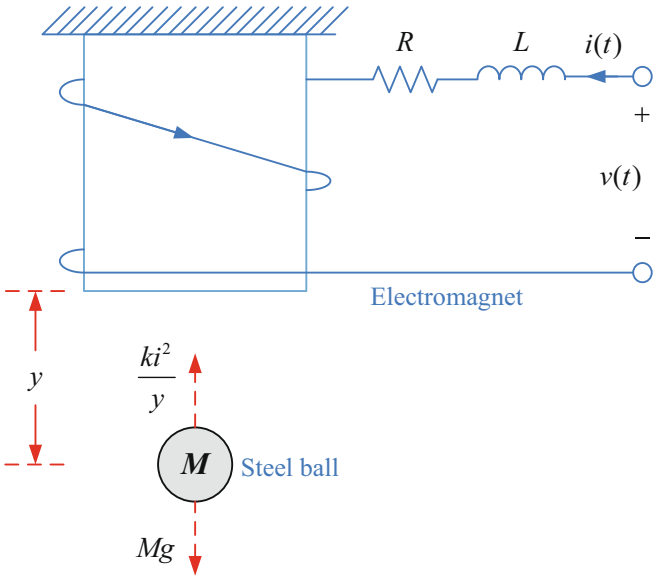


Fig. 3. Magnetic ball suspension system [35].

$$v(t) = R \cdot i(t) + L\frac{di(t)}{dt} \tag{15}$$

In here, $v(t)$ is the input voltage, L is the winding inductance and R is the winding resistance. If the state variables defined as $x_1(t) = y(t)$, $x_2(t) = dy(t)/dt$ and $x_3(t) = i(t)$, then the system's new state equations are obtained as follows.

$$\frac{dx_1(t)}{dt} = x_2(t) \tag{16}$$

$$\frac{dx_2(t)}{dt} = g - \frac{k}{M}\frac{(x_3(t))^2}{x_1(t)} \tag{17}$$

$$\frac{dx_3(t)}{dt} = -\frac{R}{L}x_3(t) + \frac{1}{L}v(t) \tag{18}$$

In the case of equilibrium, the change of position over time should be $x_{20}(t) = 0$ [35]. If these non-linear state equations are linearized around the equilibrium point of $y_0(t) = x_{10}(t) = constant$, then the equilibrium current is obtained as follows.

$$g = \frac{k}{M}\frac{(x_{30}(t))^2}{x_{10}(t)} \tag{19}$$

$$x_{30}(t) = i_0(t) = \sqrt{\frac{M \cdot g \cdot x_{10}}{k}} \tag{20}$$

The linearization is performed according to a constant value and a small disturbance value such as $x = x_0 + \Delta x$. The set of linearized equations is obtained as follows.

$$\begin{aligned} \tfrac{d\Delta x_1(t)}{dt} &= \Delta x_2(t) \\ \tfrac{d\Delta x_2(t)}{dt} &= -\tfrac{k}{M}\tfrac{2x_{30}}{x_{10}}\Delta x_3(t) + \tfrac{k}{M}\tfrac{(x_{30})^2}{(x_{10})^2}\Delta x_1(t) \\ \tfrac{d\Delta x_3(t)}{dt} &= -\tfrac{R}{L}\Delta x_3(t) + \tfrac{1}{L}\Delta v(t) \end{aligned} \tag{21}$$

$\Delta\dot{x} = A^*\Delta x + B^*\Delta u$ expresses the form of linearized state equation with the coefficient matrices A^* and B^* which are evaluated as in Eq. (22) [35].

$$A^* = \begin{bmatrix} 0 & 1 & 0 \\ \frac{g}{x_{10}} & 0 & -2\sqrt{\frac{k\cdot g}{M\cdot x_{10}}} \\ 0 & 0 & -\frac{R}{L} \end{bmatrix},\ B^* = \begin{bmatrix} 0 \\ 0 \\ 1/L \end{bmatrix} \tag{22}$$

The examined parameters of the system are listed in Table 3. If $y(t)$ is defined as the system output and $v(t)$ as the system input around the equilibrium point of $y_0(t) = 0.5m$, then by using the values in Table 3, transfer function of the system can be found with Eq. (23).

Examining Eq. (23) shows that one of the poles of the system is in the right half plane ($s_1 = -100$, $s_2 = -4.43$, $s_3 = +4.43$) meaning the open loop system is unstable. In this case, the steel ball in the uncontrolled system either sticks on to magnet or falls.

$$G(s) = C^*(sI - A^*)^{-1}B^* = [1 \quad 0 \quad 0](sI - A^*)^{-1}B^* = -\frac{885.9}{s^3 + 100s^2 - 19.62s - 1962} \tag{23}$$

Table 3
Values of magnetic ball suspension system parameters.

Parameter	Value	Unit (SI)
R	1	Ω
M	1	kg
k	1	kg-m^2/A^2-s^2
L	0.01	H
g	9.81	m/s^2

4. FOPID controller

4.1. Fundamentals of FOPID controller

Parameters known as proportional (K_p), integral (K_i) and differential (K_d) gains along with fractional integral (λ) and fractional derivative (μ) orders define a FOPID controller. The transfer function of this controller is provided as in Eq. (24) [36].

$$G_{FOPID}(s) = K_p + \frac{K_i}{s^\lambda} + K_d s^\mu,\ (\lambda, \mu > 0) \tag{24}$$

Conventional P, PI, PD, and PID controllers are special cases of FOPID controller. Graphical representation of FOPID controller is demonstrated in Fig. 4 where x and y axes represent the fractional orders of the integral and derivative terms, respectively. The latter figure is also an illustration that describes the relationship of FOPID and conventional PID controllers. As the figure shows, FOPID controller represents an extension of PID from a point to a plane. This expansion provides greater flexibility, thus, allows the achievement of real-life processes with more control accuracy [37].

4.2. Approximation of fractional differ-integrals

In practical application, numerical solutions of fractional systems must be calculated. However, it is difficult to apply fractional operators (differ-integrals) directly in the time domain. To overcome this problem, approximate methods have been adopted. The best-known approximate method belongs to Oustaloup [38]. The Oustaloup approximate method uses the recursive pole and zero distribution. The approximate transfer function is given as follows [39]

$$s^\beta \cong K \cdot \prod_{n=-N}^{N} \frac{1 + \frac{s}{\omega_{z,n}}}{1 + \frac{s}{\omega_{p,n}}},\ \beta > 0 \tag{25}$$

where K is a gain value ensuring that both sides of the Eq. (25) have a unity gain at 1 *rad/s* and $2N + 1$ is the number of pre-selected poles and zeros. Eqs. (26) and (27) provides $\omega_{z,n}$ and $\omega_{p,n}$, respectively.

$$\omega_{z,n} = \omega_b\left(\frac{\omega_h}{\omega_b}\right)^{\frac{n+N+(1-\beta)/2}{2N+1}} \tag{26}$$

$$\omega_{p,n} = \omega_b\left(\frac{\omega_h}{\omega_b}\right)^{\frac{n+N+(1+\beta)/2}{2N+1}} \tag{27}$$

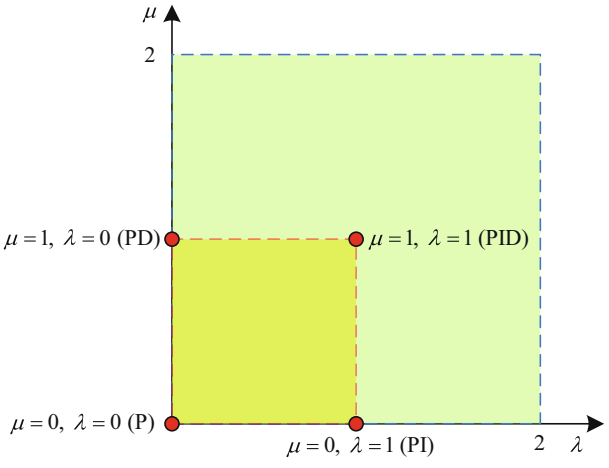


Fig. 4. FOPID controller plane.

ω_b and ω_h in the Eqs. (26) and (27) are the upper and lower frequency limits of the approximate value expressions and are generally taken as $\omega_b \cdot \omega_h = 1$, i.e. $K = {\omega_h}^{\beta}$. In this work, 11th order ($N = 5$) Oustaloup's recursive approximation is considered within the frequency bound of $\omega \in (10^{-3}, 10^{3})$ rad/s which is the most typical range in FOPID applications.

4.3. FOPID controller for magnetic ball suspension system

Magnetic ball suspension system's block diagram including FOPID controller is shown in Fig. 5. The system's closed loop transfer function (including FOPID controller) is provided in Eq. (28).

$$T(s) = \frac{G_{FOPID}(s)G(s)}{1 + G_{FOPID}(s)G(s)} = \frac{-885.9(K_d s^{\lambda+\mu} + K_p s^{\lambda} + K_i)}{(s^3 + 100s^2 - 19.62s - 1962)s^{\lambda} - 885.9(K_d s^{\lambda+\mu} + K_p s^{\lambda} + K_i)} \quad (28)$$

5. The proposed approach

5.1. The proposed objective function and FOPID controller limits

As explained in Section 3, the open loop magnetic ball suspension system is unstable by nature. The selection of the objective function is very important in finding the best values of the FOPID controller parameters used to stabilize the ball suspension system. In this study, the following new objective function is proposed as an efficient and simple structure.

$$J_{proposed} = \varphi \cdot T_s + (1 - \varphi) \cdot M_p \quad (29)$$

In here, T_s and M_p are the settling time and overshoot for unit step input, respectively. φ is the weight coefficient in the range of $(0, 1)$ that provides the coherence between settling time and overshoot. As a result of repeatedly conducted analysis, it was found that the optimum value of φ for the magnetic ball suspension system is 0.35. The upper and lower limits of the controller parameters used in this study are given as in Eq. (30) [40]. For some physical systems, controller parameters may be within negative limits [41].

$$\begin{aligned} -100 \le K_p, K_i, \text{ and } K_d \le 0 \\ 0 < \lambda, \mu < 2 \end{aligned} \quad (30)$$

5.2. Implementation of ObAEF algorithm to the magnetic ball suspension system

This section explains the proposed ObAEF-based FOPID (ObAEF-FOPID) controller presented to improve the transient response of a magnetic ball suspension system. Fig. 6 shows a detailed calculation flow chart of the ObAEF technique used to optimize the performance of the magnetic suspension system. Basically, the desired position is compared with the actual position and the obtained difference is used to feed the input of the FOPID controller. In the meantime, the actual position is also used for calculating the objective function. Then, the ObAEF is used to update the FOPID parameters. Once the optimal parameters are obtained, the system performance is verified through statistical, convergence, transient response and frequency response analyses.

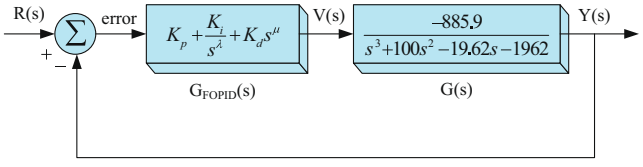


Fig. 5. Block diagram of maglev system with FOPID controller.

6. Results and discussion

The original AEF algorithm as well as the ASO and ABC algorithms were chosen for comparison in order to reveal the performance and superiority of the ObAEF technique. For detailed information on AEF, ABC and ASO algorithms, the reader can refer to refs. [20,33,34]. The coding of AEF, ObAEF, ABC and ASO algorithms, their adaptation and implementation to maglev system and all analyzes were performed by using MATLAB/Simulink (Version: 8.3) software on a personal computer with Intel® i7 2.50 GHz processor and 16.00 GB RAM. A population size of 50 for AEF, ObAEF, ABC and ASO algorithms was chosen for an appropriate comparison. The maximum number of iterations was 40 in all algorithms. The important analyzes and their results in the present study are shown in the following subsections.

6.1. Statistical results

The original AEF, ABC, ASO and the proposed ObAEF algorithms were run independently for 20 times. The statistical values of the proposed objective function ($J_{proposed}$), such as the mean, standard deviation (SD), best (min), worst (max) values are given in Table 4 and the comparative boxplot analysis results are shown in Fig. 7. The latter table and figure show that ObAEF algorithm has quite good statistical performance.

6.2. Convergence profile

The best FOPID parameters obtained after repeated runs using ABC, ASO, AEF and ObAEF algorithms are listed in Table 5. Fig. 8 shows the comparative convergence curves of $J_{proposed}$ objective function used in the optimization of FOPID parameters of magnetic ball suspension system versus the number of iterations. As can be seen from the figure, the improved algorithm (ObAEF) reached the lowest $J_{proposed}$ value with minimal iterations (at 13th iteration) whilst ABC, ASO and AEF algorithms have reached their lowest values in 18th, 20th and 23rd iterations, respectively.

If the optimal FOPID controller parameters in Table 5 are used in Eq. (28), the closed loop transfer functions of the magnetic suspension system with ABC-FOPID, ASO-FOPID, AEF-FOPID and ObAEF-FOPID controllers given in Eqs. (31) - (34) are obtained, respectively.

$$T_{ABC} = \frac{4516.5s^{2.0198} + 74235s^{0.9905} + 68512}{s^{3.9905} + 100s^{2.9905} + 4516.5s^{2.0198} - 19.62s^{1.9905} + 72273s^{0.9905} + 68512} \quad (31)$$

$$T_{ASO} = \frac{2406.6s^{2.0443} + 43853s^{0.8845} + 61973}{s^{3.8845} + 100s^{2.8845} + 2406.6s^{2.0443} - 19.62s^{1.8845} + 41891s^{0.8845} + 61973} \quad (32)$$

$$T_{AEF} = \frac{3201.5s^{2.1308} + 64547s^{0.9812} + 71783}{s^{3.9812} + 100s^{2.9812} + 3201.5s^{2.1308} - 19.62s^{1.9812} + 62585s^{0.9812} + 71783} \quad (33)$$

$$T_{ObAEF} = \frac{2835.2s^{2.0172} + 72722s^{0.7769} + 84770}{s^{3.7769} + 100s^{2.7769} + 2835.2s^{2.0172} - 19.62s^{1.7769} + 70760s^{0.7769} + 84770} \quad (34)$$

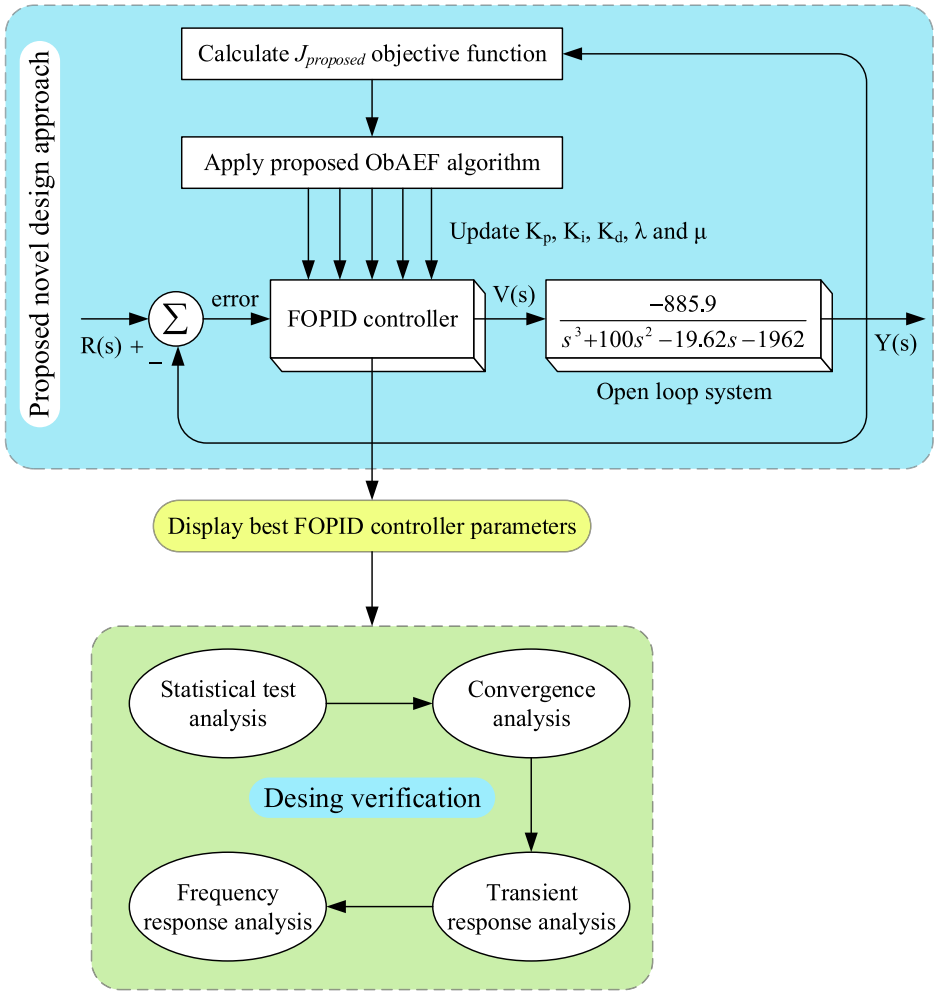


Fig. 6. ObAEF application block diagram for magnetic ball suspension system.

Table 4
Statistical values of $J_{proposed}$.

Statictical Index	ABC	ASO	AEF	ObAEF
Mean	0.3158	0.2817	0.2424	0.2028
SD	0.0153	0.0139	0.0182	0.0040
Best	0.3015	0.2620	0.2271	0.1971
Worst	0.3531	0.3104	0.2854	0.2088

6.3. Transient response

The transient responses of the system to a reference position change of $\Delta y = 5$ cm around the equilibrium point of $y_0 = 0.5$ m for ABC-FOPID, ASO-FOPID, AEF-FOPID and ObAEF-FOPID controllers are shown in Fig. 9. Also, comparative numerical results in terms of maximum overshoot, rise time ($10\% \rightarrow 90\%$) and settling time ($\pm 2\%$ band) are presented in Table 6. Considering the comparative transient response analysis results in Fig. 9 and Table 6, all the performance criteria such as overshoot, rise time and settling time have reached the lowest values with the proposed ObAEF-FOPID controller designed for magnetic ball suspension system. These results confirm the superiority of the ObAEF algorithm in terms of strong global and local search capabilities since it improves the transient response of the system.

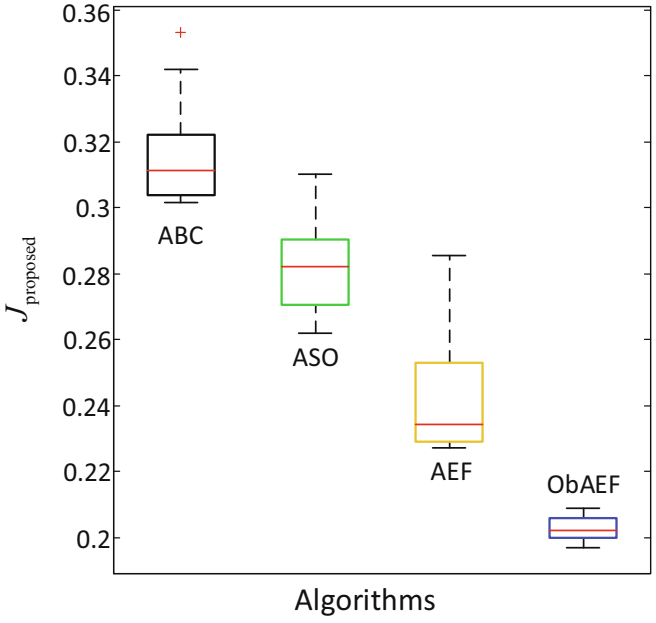


Fig. 7. Boxplot analysis results for ABC, ASO, AEF and proposed ObAEF algorithms.

Table 5
Tuned FOPID controller parameters.

Controller	K_p	K_i	λ	K_d	μ
ABC-FOPID	−83.7975	−77.3375	0.9905	−5.0983	1.0293
ASO-FOPID	−49.5017	−69.9558	0.8845	−2.7166	1.1598
AEF-FOPID	−72.8609	−81.0298	0.9812	−3.6139	1.1496
ObAEF-FOPID	−82.0892	−95.6888	0.7769	−3.2004	1.2403

Table 6
Comparative transient response analysis results of magnetic ball suspension system.

Controller	Maximum overshoot (%)	Settling time (s)	Rise time (s)
ABC-FOPID	27.8227	0.3448	0.0246
ASO-FOPID	21.1222	0.3562	0.0328
AEF-FOPID	17.1741	0.3300	0.0257
ObAEF-FOPID	**14.8608**	**0.2873**	**0.0233**

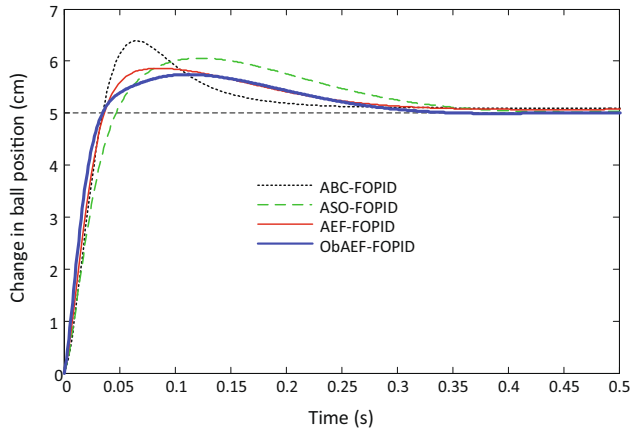


Fig. 9. Comparative closed-loop system responses to a step change of $\Delta y = 5$ cm.

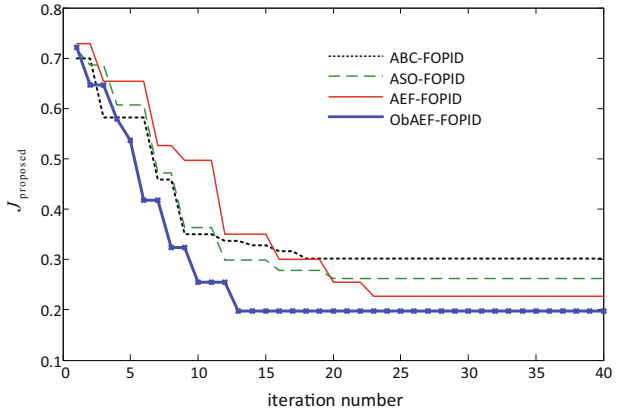


Fig. 8. Convergence profiles of ABC, ASO, AEF and proposed ObAEF algorithms.

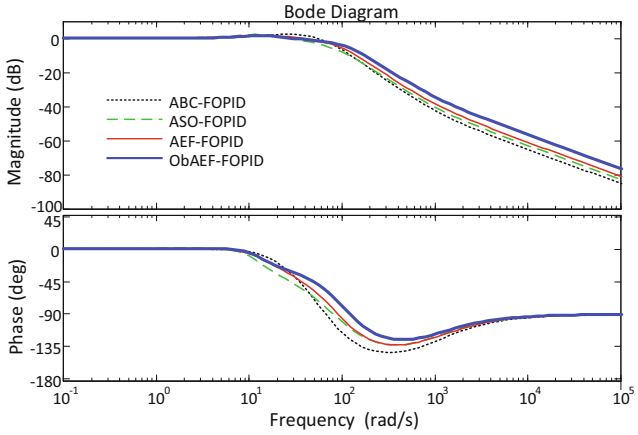


Fig. 10. Bode plot of magnetic ball suspension system with different controllers.

6.4. Frequency response

The gain margin, phase margin and bandwidth were calculated from the Bode diagram. High gain and phase margins are indication of good frequency response stability. Also, a high bandwidth provides a lower rise time to a system. Fig. 10 shows the comparative Bode diagram of the magnetic ball suspension system with ABC-FOPID, ASO-FOPID, AEF-FOPID and ObAEF-FOPID controllers. Comparative frequency response performance criteria are presented numerically in Table 7. As can clearly be seen from the table, the proposed ObAEF-FOPID controller provides the most stable system in terms of frequency response.

Table 7
Comparative Bode analysis results of magnetic ball suspension system.

Controller	Gain margin (dB)	Phase margin (deg.)	Bandwidth (Hz)
ABC-FOPID	∞	103.2657	75.3558
ASO-FOPID	∞	134.5349	54.6252
AEF-FOPID	∞	133.2568	73.7792
ObAEF-FOPID	∞	**147.1847**	**84.8300**

6.5. Comparison with the state-of-the-art algorithms

In order to confirm the efficiency of ObAEF-FOPID controller, the obtained transient and frequency responses were compared with other optimization algorithms that are available in the literature regarding magnetic ball suspension system having the same parameters and adopting PID controller. Those algorithms are sine cosine (SCA) [40], wind driven optimization (WDO) [40], whale optimization (WOA) [42] and simulated annealing (SA) [42] algorithms. A comparison of transient and frequency response analyses including maximum overshoot, settling time, rise time, gain margin, phase margin and bandwidth are presented in Table 8. As can clearly be observed from Table 8, the proposed ObAEF-FOPID controller provides better system output in terms of time and frequency domain responses.

Table 8
Comparison of transient and frequency responses.

Controller	Transient response stability parameters			Frequency response stability parameters		
	Maximum overshoot (%)	Settling time (s)	Rise time (s)	Gain margin (dB)	Phase margin (deg.)	Bandwidth (Hz)
ObAEF-FOPID	14.8608	0.2873	0.0233	∞	147.1847	84.8300
SCA-PID [40]	24.8724	0.5506	0.0168	∞	84.3857	117.7911
WDO-PID [40]	26.1061	0.5735	0.0185	∞	87.1318	105.9398
WOA-PID [42]	28.6102	0.5089	0.0334	∞	107.1484	54.2521
SA-PID [42]	44.0653	0.6031	0.0358	∞	85.5659	47.4373

7. Conclusion

In this study, ObAEF technique was proposed for the first time ever for the design of FOPID controller in magnetic ball suspension system with a new objective function. In order to reveal the effectiveness of the proposed approach, it was first applied to six well-known benchmark optimization problems and the results were compared with other algorithms. The best statistical results of these test functions, in terms of mean, standard deviation, worst and best values, were found with ObAEF whilst compared to basic AEF along with ABC and ASO algorithms. An ObAEF based FOPID controller was also designed for improving the transient response of a maglev system. Thus, further performance comparisons with the same algorithms were performed through convergence profile, statistical success, transient and frequency responses. The simulation results have revealed that the FOPID controller designed for the magnetic ball suspension system tuned by using a new, simple structure objective function with the proposed ObAEF technique has achieved the best performance criteria such as maximum overshoot, settling time, rise time, gain margin, phase margin and bandwidth. Hence, the proposed tuning approach is superior and effective than those compared methods and is a promising approach for being applied to other real-world engineering problems such as automatic voltage regulator system design, DC motor speed and position control etc., which can be the matter of our future studies.

Declaration of Competing Interest

The authors declare that they have no known competing financial interests or personal relationships that could have appeared to influence the work reported in this paper.

References

[1] M. Moazen, M.B.B. Sharifian, H. Afshari, PID control of Maglev Guiding System for Linear Elevator, in: 2012 IEEE 5th India Int. Conf. Power Electron., 2012: pp. 1–6. https://doi.org/10.1109/IICPE.2012.6450409.

[2] H. Zhou, J. Duan, Levitation mechanism modelling for maglev transportation system, J. Cent. South Univ. Technol. 17 (2010) 1230–1237, https://doi.org/10.1007/s11771-010-0624-z.

[3] T. Mizuno, M. Takasaki, D. Kishita, K. Hirakawa, Vibration isolation system combining zero-power magnetic suspension with springs, Control Eng. Pract. 15 (2007) 187–196, https://doi.org/10.1016/j.conengprac.2006.06.001.

[4] W. Yu, P.C. Francisco, X. Li, Two-stage neural sliding-mode control of magnetic levitation in minimal invasive surgery, Neural Comput. Appl. 20 (2011) 1141–1147, https://doi.org/10.1007/s00521-010-0477-2.

[5] I. Ahmad, M. Shahzad, P. Palensky, Optimal PID control of Magnetic Levitation System using Genetic Algorithm, in: 2014 IEEE Int. Energy Conf., 2014: pp. 1429–1433. https://doi.org/10.1109/ENERGYCON.2014.6850610.

[6] V. Mohan, H. Chhabra, A. Rani, V. Singh, An expert 2DOF fractional order fuzzy PID controller for nonlinear systems, Neural Comput. Appl. 31 (2019) 4253–4270, https://doi.org/10.1007/s00521-017-3330-z.

[7] E. Çelik, N. Öztürk, First application of symbiotic organisms search algorithm to off-line optimization of PI parameters for DSP-based DC motor drives, Neural Comput. Appl. 30 (2018) 1689–1699, https://doi.org/10.1007/s00521-017-3256-5.

[8] B. Hekimoğlu, S. Ekinci, Grasshopper optimization algorithm for automatic voltage regulator system, in: 2018 5th Int. Conf. Electr. Electron. Eng. ICEEE 2018, 2018: pp. 152–156. https://doi.org/10.1109/ICEEE2.2018.8391320.

[9] E. Çelik, R. Durgut, Performance enhancement of automatic voltage regulator by modified cost function and symbiotic organisms search algorithm, Eng. Sci. Technol. Int. J. 21 (2018) 1104–1111, https://doi.org/10.1016/j.jestch.2018.08.006.

[10] B. Hekimoğlu, Optimal Tuning of Fractional Order PID Controller for DC Motor Speed Control via Chaotic Atom Search Optimization Algorithm, IEEE Access. 7 (2019) 38100–38114, https://doi.org/10.1109/ACCESS.2019.2905961.

[11] D. Sain, Real-Time implementation and performance analysis of robust 2-DOF PID controller for Maglev system using pole search technique, J. Ind. Inf. Integr. 15 (2019) 183–190, https://doi.org/10.1016/j.jii.2018.11.003.

[12] A. Ghosh, T. Rakesh Krishnan, P. Tejaswy, A. Mandal, J.K. Pradhan, S. Ranasingh, Design and implementation of a 2-DOF PID compensation for magnetic levitation systems, ISA Trans. 53 (2014) 1216–1222, https://doi.org/10.1016/j.isatra.2014.05.015.

[13] S.K. Swain, D. Sain, S.K. Mishra, S. Ghosh, Real time implementation of fractional order PID controllers for a magnetic levitation plant, AEU - Int. J. Electron. Commun. 78 (2017) 141–156, https://doi.org/10.1016/j.aeue.2017.05.029.

[14] D. Sain, S.K. Swain, S.K. Mishra, Real Time Implementation of Optimized I-PD Controller for the Magnetic Levitation System using Jaya Algorithm, IFAC-PapersOnLine. 51 (2018) 106–111, https://doi.org/10.1016/j.ifacol.2018.05.018.

[15] C. Thammarat, S. Hlangnamthip, D. Puangdownreong, Optimizing PID Controller Design for Maglev Air-Gap Position Control by Bat-Inspired Algorithm, in: 2019 Jt. Int. Conf. Digit. Arts, Media Technol. with ECTI North. Sect. Conf. Electr. Electron. Comput. Telecommun. Eng. (ECTI DAMT-NCON), 2019: pp. 282–285. https://doi.org/10.1109/ECTI-NCON.2019.8692261.

[16] S. Yadav, S.K. Verma, S.K. Nagar, Performance enhancement of magnetic levitation system using teaching learning based optimization, Alexandria Eng. J. 57 (2018) 2427–2433, https://doi.org/10.1016/j.aej.2017.08.016.

[17] A.S. Chopade, S.W. Khubalkar, A.S. Junghare, M.V. Aware, S. Das, Design and implementation of digital fractional order PID controller using optimal pole-zero approximation method for magnetic levitation system, IEEE/CAA J. Autom. Sin. 5 (2018) 977–989, https://doi.org/10.1109/JAS.2016.7510181.

[18] P. Roy, M. Borah, L. Majhi, N. Singh, Design and implementation of FOPID controllers by PSO, GSA and PSOGSA for MagLev system, in: 2015 Int. Symp. Adv. Comput. Commun. ISACC 2015, 2016: pp. 10–15. https://doi.org/10.1109/ISACC.2015.7377307.

[19] G. Altintas, Y. Aydin, A comparison on genetic algorithm based integer order and fractional order PID control of magnetic bearing system, in: 2017 IEEE Int. Conf. Mechatronics, 2017: pp. 20–24. https://doi.org/10.1109/ICMECH.2017.7921074.

[20] Anita, A. Yadav, AEFA: Artificial electric field algorithm for global optimization, Swarm Evol. Comput. 48 (2019) 93–108. https://doi.org/10.1016/j.swevo.2019.03.013.

[21] A. Anita, N. Yadav, Kumar, Artificial electric field algorithm for engineering optimization problems, Expert Syst. Appl. 149 (2020), https://doi.org/10.1016/j.eswa.2020.113308 113308.

[22] A. Anita, Yadav, Discrete artificial electric field algorithm for high-order graph matching, Appl. Soft Comput. 92 (2020), https://doi.org/10.1016/j.asoc.2020.106260 106260.

[23] H.R. Tizhoosh, Opposition-Based Learning: A New Scheme for Machine Intelligence, in: Int. Conf. Comput. Intell. Model. Control Autom. Int. Conf. Intell. Agents, Web Technol. Internet Commer., 2005: pp. 695–701. https://doi.org/10.1109/CIMCA.2005.1631345.

[24] M. Abd Elaziz, D. Oliva, S. Xiong, An improved Opposition-Based Sine Cosine Algorithm for global optimization, Expert Syst. Appl. 90 (2017) 484–500, https://doi.org/10.1016/j.eswa.2017.07.043.

[25] M. Abd Elaziz, D. Oliva, Parameter estimation of solar cells diode models by an improved opposition-based whale optimization algorithm, Energy Convers. Manag. 171 (2018) 1843–1859, https://doi.org/10.1016/j.enconman.2018.05.062.

[26] R.A. Ibrahim, M.A. Elaziz, D. Oliva, E. Cuevas, S. Lu, An opposition-based social spider optimization for feature selection, Soft Comput. 23 (2019) 13547–13567, https://doi.org/10.1007/s00500-019-03891-x.

[27] M. Pradhan, P.K. Roy, T. Pal, Oppositional based grey wolf optimization algorithm for economic dispatch problem of power system, Ain Shams Eng. J. 9 (2018) 2015–2025, https://doi.org/10.1016/j.asej.2016.08.023.

[28] X. Bao, H. Jia, C. Lang, Dragonfly algorithm with Opposition-based learning for multilevel thresholding color image segmentation, Symmetry (Basel). 11 (2019), https://doi.org/10.3390/sym11050716.

[29] P. Jain, A. Saxena, An opposition theory enabled moth flame optimizer for strategic bidding in uniform spot energy market, Eng. Sci. Technol. Int. J. 22 (2019) 1047–1067, https://doi.org/10.1016/j.jestch.2019.03.005.

[30] M. Tubishat, N. Idris, L. Shuib, M.A.M. Abushariah, S. Mirjalili, Improved Salp Swarm Algorithm based on opposition based learning and novel local search algorithm for feature selection, Expert Syst. Appl. 145 (2020), https://doi.org/10.1016/j.eswa.2019.113122 113122.
[31] S. Ekinci, A. Demiroren, H. Zeynelgil, B. Hekimoğlu, An opposition-based atom search optimization algorithm for automatic voltage regulator system, J. Fac. Eng. Archit. Gazi Univ. 35 (2020) 1141–1158. https://doi.org/10.17341/gazimmfd.598576.
[32] S. Shekhawat, A. Saxena, Development and applications of an intelligent crow search algorithm based on opposition based learning, ISA Trans. 99 (2020) 210–230. https://doi.org/https://doi.org/10.1016/j.isatra.2019.09.004.
[33] D. Karaboga, B. Basturk, A powerful and efficient algorithm for numerical function optimization: Artificial bee colony (ABC) algorithm, J. Glob. Optim. 39 (2007) 459–471, https://doi.org/10.1007/s10898-007-9149-x.
[34] W. Zhao, L. Wang, Z. Zhang, Atom search optimization and its application to solve a hydrogeologic parameter estimation problem, Knowledge-Based Syst. 163 (2019) 283–304, https://doi.org/10.1016/j.knosys.2018.08.030.
[35] B.C. Kuo, Automatic control systems, 8th ed.., John Wiley & Sons, New York, 2003.
[36] A. Ateş, C. Yeroglu, Optimal fractional order PID design via Tabu Search based algorithm, ISA Trans. 60 (2016) 109–118, https://doi.org/10.1016/j.isatra.2015.11.015.
[37] P. Shah, S. Agashe, Review of fractional PID controller, Mechatronics. 38 (2016) 29–41. https://doi.org/10.1016/j.mechatronics.2016.06.005.
[38] A. Oustaloup, F. Levron, B. Mathieu, F.M. Nanot, Frequency-band complex noninteger differentiator: Characterization and synthesis, IEEE Trans. Circuits Syst. I Fundam. Theory Appl. 47 (2000) 25–39, https://doi.org/10.1109/81.817385.
[39] J. Morsali, K. Zare, M. Tarafdar Hagh, Applying fractional order PID to design TCSC-based damping controller in coordination with automatic generation control of interconnected multi-source power system, Eng. Sci. Technol. Int. J. 20 (2017) 1–17, https://doi.org/10.1016/j.jestch.2016.06.002.
[40] C. Ozaydin, H.L. Zeynelgil, S. Ekinci, B. Hekimoglu, PID Controller Design Based on Sine Cosine Algorithm for Magnetic Ball Suspension System, in: 2019 Int. Conf. Artif. Intell. Data Process. Symp. IDAP 2019, 2019: pp. 1–7. https://doi.org/10.1109/IDAP.2019.8875938.
[41] R.C. Dorf, Modern control systems, 12th ed., Boston; London, Pearson, 2011.
[42] S. Ekinci, A. Demiroren, B. Hekimoglu, E. Eker, Performance Enhancement of Magnetic Ball Suspension System Using Hybrid Whale Optimization Algorithm with Simulated Annealing, in: 3rd Int. Symp. Multidiscip. Stud. Innov. Technol. ISMSIT 2019 - Proc., IEEE, 2019: pp. 1–6. https://doi.org/10.1109/ISMSIT.2019.8932787.